Journal of Imaging Science and Technology® 51(1): 61–69, 2007.

Development of a Multi-spectral Scanner using LED Array for Digital Color Proof

Shoji Yamamoto, Norimichi Tsumura and Toshiya Nakaguchi
Department of Information and Image Sciences, Chiba University, Yayoi-cho, Inage-ku, Chiba, 263-8522, Japan

Yoichi Miyake
Research Center for Frontier Medical Engineering, Chiba University, Yayoi-cho, Inage-ku, Chiba, 263-8522, Japan
E-mail: yamasho@graduate.chiba-u.jp

Abstract. *The authors have developed a multi-spectral scanner for accurately printing proofs that employs an LED array coupled with a photodiode array to measure the reflectance spectra. The system is composed of an LED array with five different spectral radiant distributions and 2048 silicon photodiodes with a Selfoc lens array (SLA) for imaging. Five types of LED were selected from among 40 types of commercially available LED with different spectral radiant distributions in order to minimize the average color difference ΔE^*_{94} between the measured and estimated reflectance spectra of 81 typical color charts. The multiple regression method based on the clustering and polynomial regression algorithm was introduced for highly accurate estimation of the spectral reflectance for printing. The results indicate that the average and maximum color differences ΔE^*_{94} between the measured and estimated reflectance spectra of 928 color charts were 1.02 and 2.84, respectively. The scanner can measure the reflectance of prints having a* 0.5 mm *pitch resolution and a scanning speed of* 100 mm/s. *The field programmable gate array (FPGA) and digital signal processor (DSP) were introduced in order to accelerate the calculation of sensor calibration and the estimation of the reflectance spectra of the printed proof for practical and commercial use. As a result, the developed scanner could measure the reflectance spectra of the printed proof within* 20 s.

[DOI: 10.2352/J.ImagingSci.Technol.(2007)51:1(61)]

INTRODUCTION

Color proofing has been widely used to evaluate and consider the color reproduction in printing, in order to provide a guarantee to customers regarding the quality of print based on the colorimetric color reproduction. In recent years, the availability of accurate digital color proofs via computer networks has reduced the cost and time associated with transportation.[1,2]

A color densitometry scanner is usually used to measure and digitize the color information of the color proof into R, G, B densities.[3–5] Printing proofs based on densitometric measurement are influenced by the illuminantion condition. For colorimetric color reproduction in the printing industry, it is necessary to compare color proofs and prints under the illuminant D50.[6,7] In the process of gaining approval by the customer, however, the use of D50 is not always practical.

Recently, multi-spectral imaging[8–15] has been developed for accurate color reproduction under different illuminants. The reflectance spectra of the object are acquired in this imaging system for calculating the colorimetric values under arbitrary illuminants. Multi-spectral imaging is usually performed using five or more color filters for multi-band imaging. Typically, rotating filters are mounted in front of a monochrome CCD camera.[8–11] However, a great deal of time is required to rotate the filters with a mechanical wheel. Therefore, instead of rotating filters, a liquid crystal tunable filter (LFTF) may be used in multi-spectral imaging.[12–14] This is appropriate for high speed measurement because the LFTF can change the spectral distribution of the filter, such as the peak wavelength and bandwidth, within several milliseconds. As a recently developed method for high-speed measurement, the CRISTATEL project[15] uses a small cask with filters and a linear CCD array detector, which provides 10 ms scanning for each filter. However, these methods require a distance of more than 30 cm between the device and the object, which is not practical for factory use. In addition, it is necessary to satisfy the specifications of accuracy, compactness, and high speed measurement for creating digital color proofs in the print industry.

We developed a multi-spectral scanner using an LED array and a photodiode array in order to accurately measure the spectral characteristics of the printing proof. A compact scanner can be achieved using LED illumination and an optical element, such as the Selfoc lens array. Conventional color filters are not necessary in this scanner because the LED emits light that has a band-limited spectral radiant distribution. Since the LED response time is very fast, high-speed measurement is possible by the timesharing control of each LED emission.

In designing the multi-spectral scanner with an LED array, it is important to decide the number of LEDs and the spectral radiant distribution of each LED. The algorithm by which to decide the optimal combination of LEDs is explained in the third section. We develop the multi-spectral

Received Jul. 3, 2005; accepted for publication Oct. 2, 2006.
1062-3701/2007/51(1)/61/9/$20.00.

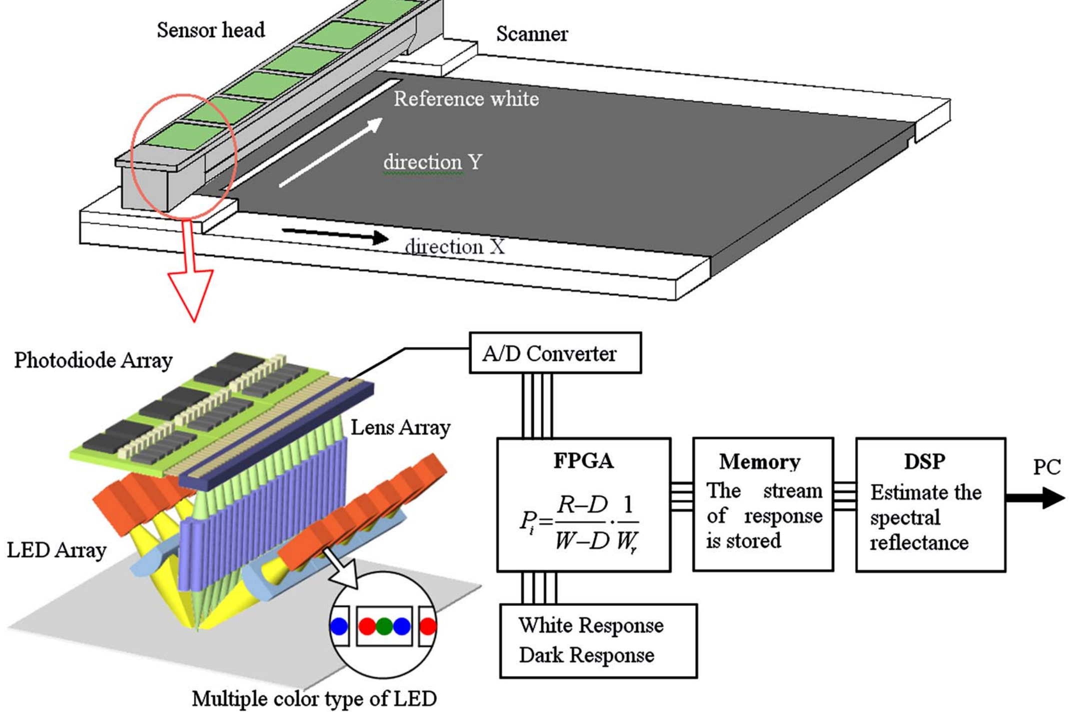

Figure 1. Schematic illustration of the multi-spectral scanner using an LED array.

scanner using the obtained optimal combination of LEDs and evaluate the accuracy of estimated reflectance spectra in the fourth and fifth sections, respectively. In order to improve the accuracy of the estimation, we also introduce additional algorithms using the clustering method and the polynomial regression method in the sixth section. Finally, concluding remarks are presented in the seventh section.

COMPACT MULTI-SPECTRAL SCANNER USING AN LED ARRAY

Figure 1 shows a schematic design of the proposed multi-spectral scanner. In order to satisfy the geometric conditions defined by the ISO or DIN standard[6] for the 0–45° method, the LED array is attached to a mount in order to illuminate the print from 45°, and the detector array is set to detect the light at 0° from the print. The Selfoc lens array (SLA) is inserted between the print and the detector in order to achieve a compact structure.

In this system, a multiple-color type LED is used for multi-spectral imaging. Each emission for color can be controlled independently in this multiple-color LED. The analog responses of the photodetector for each color emission in the LED are converted to digital values, and the calibrated value $P_i(x,y)$ at position (x,y) illuminated by the ith LED is expressed as

$$P_i(x,y) = \frac{\int_{380}^{780} S(\lambda)L_i(y,\lambda)R(x,y,\lambda)\,d\lambda - D(y)}{\int_{380}^{780} S(\lambda)L_i(y,\lambda)W(y,\lambda)\,d\lambda - D(y)} \frac{1}{Wr_i}, \quad (1)$$

where $S(\lambda)$ is the spectral sensitivity of the photodiode, $R(\lambda)$ is the spectral reflectance of the print, and $L_i(y,\lambda)$ is the spectral radiant distribution of the ith LED at position y. The spectral reflectance $W(y,\lambda)$ is measured on the reference white plate at position y, and $D(y)$ is the measured response of the photodiode when all of the LEDs are switched off. The coefficient Wr_i is used to compensate the difference between the reference white plate and the standard white corresponding to the ith LED. The practical use of the LED for color measurement requires two compensations, one for amplitude fluctuation and one for wavelength fluctuation. Equation (1) indicates a compensation for the amplitude fluctuation of the LED. A compensation for the wavelength fluctuation is taken into account in the LED selection in the third section. Equation (1) is applied for a large number of photodiodes in the multi-spectral scanner. In our system, we use a field programmable gate array (FPGA) for calculation because the FPGA has can perform a large number of simple, high-speed calculations.

As mentioned above, each color emission in the LED is controlled by the timesharing process, and the responses of the photodetector for color emissions are ordered and

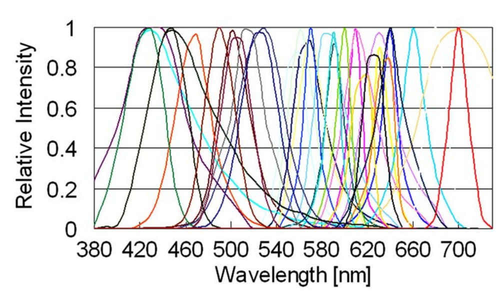

Figure 2. Spectral radiant distribution of commercially available LEDs.

streamed in the time series. The stream of responses is stored in memory for each set of color emissions in the pixel. Based on the stored set of color emissions, the spectral reflectance is estimated in the digital signal processor (DSP). The DSP is superior for calculating vector-matrix operation at high speed, i.e., for handling the stored responses in the memory. In the present paper, the multiple regression method is used for spectral estimation.[9] The estimation process for the multiple regression method is expressed simply as follows:

$$\begin{bmatrix} \hat{R}_{380} \\ \hat{R}_{390} \\ \vdots \\ \hat{R}_{780} \end{bmatrix} = \begin{bmatrix} A_{380,1} & A_{380,2} & \cdots & A_{380,i} \\ A_{390,1} & \ddots & & \\ \vdots & & & \vdots \\ A_{780,1} & & \cdots & A_{780,i} \end{bmatrix} \begin{bmatrix} P_1 \\ P_2 \\ \vdots \\ P_i \end{bmatrix}, \tag{2}$$

where $\hat{R}_\lambda$ is the estimated reflectance at wavelength λ, and $A_{\lambda,i}$ are the elements of the estimation matrix, which is determined from the relationship between the scanner response and the spectral reflectance of the samples. The sample should be chosen so as to represent the target prints and should be measured *a priori*.

SELECTION OF LEDs

In developing a multi-spectral scanner using an LED array, it is important to decide the number of LEDs and the spectral radiant distribution of the LEDs. In conventional multi-spectral imaging using the color filters, it is possible to optimize the spectral distribution of the filters[9] and produce the optimized filters in industry. However, the spectral radiant distribution of the LED has already been decided by the epitaxy process of the LED. Thus, it is not practical to optimize the spectral radiant distribution of the LED when designing the imaging system. In the present paper, we selected an LED combination from 40 types of commercially available LEDs in order to minimize the error between the original reflectance and the estimated reflectance. Figure 2 shows the spectral radiant distributions of the LEDs, which are normalized by the peak power and are obtained from the specifications of the LED. However, the peak wavelength of each LED is usually shifted by the fluctuations in the epitaxial deposition process during manufacture. Figure 3 shows typical examples of this fluctuation. This fluctuation must be taken into account in order to select the LEDs for robust design in the imaging system.

In the following, we will explain the flow of the LED selection for the optimized robust imaging system. In the first step, the number of LEDs to be selected is i, and the flow is repeated while varying i from 3 to 7, in order to decide the optimal number of LEDs. Here, n is the combination of 40 items taken i at a time, and the evaluation process is repeated n times by changing the combination of LEDs.

Next, the responses for the reflectance sample illuminated by the LED combination are obtained by computer simulation of the imaging system, and the calibrated responses are obtained by Eq. (1). The spectral reflectance is estimated from the calibrated responses by using the multiple regression method, as given by Eq. (2). The noise generated by the photo detector is usually added in the optimization process of the multiple regression method. However, this noise is ignored in our selection of the optimal LED because our system has a circuit for the compensation of the signal-to-noise ratio, as shown below in the fourth section. This circuit can provide an adequate signal-to-noise ratio by controlling the radiation time of the LED, even if a narrow-band LED is selected.

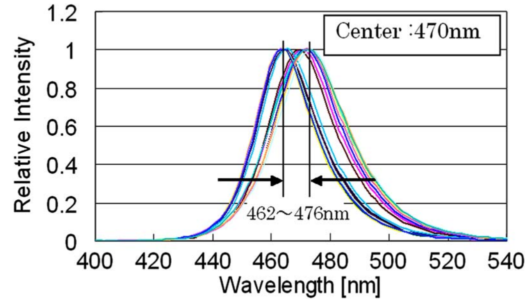

Figure 3. Example of the shift of peak wavelength generated in the epitaxial deposition manufacturing process.

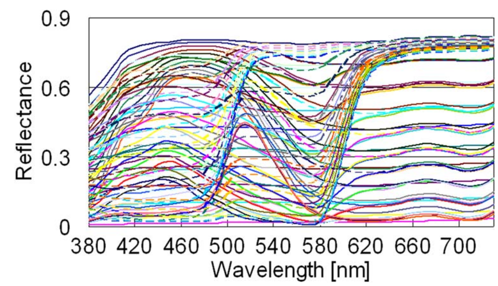

Figure 4. Reflectance spectra of 81 color samples printed on coated paper.

If the color difference between the measured reflectance and the estimated reflectance is greater than the permissible threshold, then the calculation progresses to the next evaluation process by changing the combination of LEDs. In addition, if the color difference is equal to or less than a permissible threshold, the color difference value and the combination of LEDs are recorded.

The estimated reflectance is evaluated in comparison with the original reflectance of the sample. In the present paper, 81 samples for reflectance are examined for each evaluation of the LED combinations. These samples are halftone printed samples and white paper. The halftone samples have dot areas ranging from 10% to 100% in 10% pitches of C, M, Y, K, MY, CY, CM, and CMY, respectively. Figure 4 shows the reflectance spectra of the 81 color samples, which are printed on coated paper and measured by a portable spectrophotometer (Gretag-Machbeth Spectro-Eye). The choice of these samples is related to the application of the digital color proof for offset print.

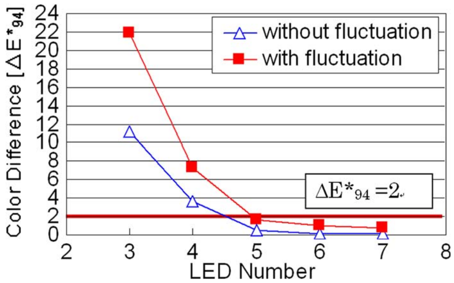

Figure 5. Results of simulation for various numbers of LEDs (D50 illuminant).

The criteria for evaluation should be set so as to meet the criteria used in practical applications for various types of papers and illuminants. For the criteria in the present paper, we first optimized the LED selection by using illuminant D50 and coated paper, which is the most popular combination in the graphics industry and is defined in ISO 13655.[6] The criteria for other paper and illuminant combinations were evaluated using the optimal combination of LEDs, which was selected using illuminant D50 and coated paper.

It is also necessary at evaluation to consider the fluctuation of the peak wavelength for the criteria. When the color difference ΔE^*_{94} in the CIE $L^*a^*b^*$ color space[16] is equal to or less than a permissible threshold in the evaluation process, we add a ±10 nm variation to the peak wavelength for each LED in the process of estimation. The degree of variation of ±10 nm is decided with a sufficient range from the measurements of LEDs, as shown in Fig. 3. Since the variations of −10 nm, 0 nm, and +10 nm should be applied to each LED, we have 3^i variations for i LEDs. The maximum color difference ΔE^*_{94} indicates the maximum value obtained by the calculated results of 3^i types of variation, which has −10 nm, 0 nm, and +10 nm fluctuations of peak wavelength at each LED, respectively. Finally, the maximum color difference ΔE^*_{94} is used for the final evaluation value of the current combination of LEDs.

Figure 5 shows the results of calculation for the variation of the number of LEDs. In this figure, the triangles indicate the result of the maximum ΔE^*_{94} without the ±10 nm fluctuation of the peak wavelength, and the squares indicate the results of the maximum ΔE^*_{94}, which was used for robust assessment of the ±10 nm fluctuation. Both results indicate that the accuracy of estimation is improved as the number of LEDs increases. Five LEDs are necessary in order to estimate a spectral reflectance below the maximum $\Delta E^*_{94}=2$, which is calculated between the original reflectance spectra and the estimated reflectance spectra. Figure 6 shows the spectral radiant distributions of the best combination for three, four, five and six LEDs. The best number of LEDs was determined to be 5, and the peak wavelengths of the LEDs were obtained as 450, 470, 530, 570, and 610 nm, respectively.

As mentioned above, five LEDs were determined to be effective for various printed papers and illuminant conditions, although the best selection was obtained by evaluation using only illuminant D50. We next evaluate the effectiveness of the estimation in detail. Table I shows the printed paper and illuminant conditions that are used to verify the influences of the printed paper and illuminant conditions on the estimation. The accuracy of the estimation is examined using "art paper" and "matte paper," which are often used in the print industry. The estimation matrix is calculated using 81 color samples of "coated paper" prints under the illuminant D50, as mentioned above, and the spectral reflectance is estimated from the response of the multi-spectral scanner for art and matte color samples. The accuracy of the estimation is also examined under A, C, D50, and D65. Figure 7 and Table II show the results as maximum ΔE^*_{94} between the

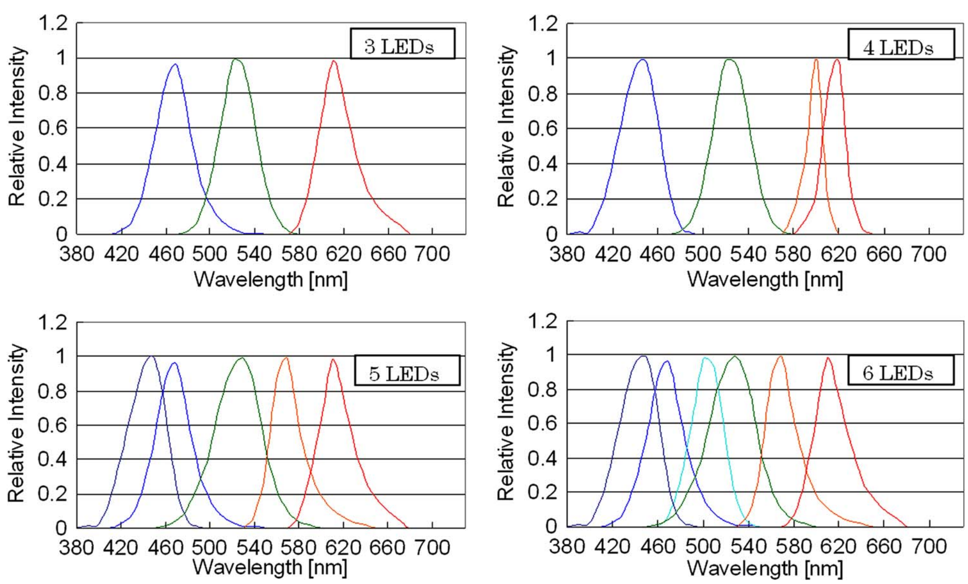

Figure 6. Spectral radiance distribution of LEDs obtained by simulation using an LED array.

Table I. Calculation conditions verified by the influence of the printed paper and the illuminant an LED array.

LED No.	Printed paper	Illuminant
	Condition 1	
5	Coat	D50
5	Art	D50
5	Matte	D50
	Condition 2	
5	Coat	A
5	Coat	C
5	Coat	D50
5	Coat	D65

Table II. Results for maximum ΔE^*_{94} between the original reflectance and the estimated reflectance for each paper and illuminant.

Condition		Color difference ΔE^*_{94}	
Printed paper	Illuminant	Without fluctuation	With fluctuation
Coat	D50	0.48	1.52
Art	D50	0.44	1.51
Matte	D50	0.28	0.89
Coat	A	0.52	1.55
Coat	C	0.50	1.53
Coat	D50	0.49	1.52
Coat	D65	0.44	1.52

original reflectance and estimated reflectance in 81 color samples for each paper and illuminant. Note that the estimated reflectance for this result is calculated using the best selection among 450, 470, 530, 570, and 610 nm LEDs, which are obtained with illuminant D50 and coated paper.

The black bar in this graph shows the results for maximum ΔE^*_{94} without ±10 nm fluctuation of peak wavelength, and the gray bar shows the results for maximum ΔE^*_{94} with ±10 nm fluctuation of the peak wavelength. In Fig. 7(a), the estimation accuracies for art and matte papers are higher than that for coated paper, even if the estimation matrix was designed for coated paper. In general, the accuracy of estimation depends on the spectral gamut range, which is the low-dimensional linear space calculated by principal component analysis with training samples. Since the spectral gamut ranges of colors on art and matte papers are included within the spectral gamut range of colors on coated paper because of ink/media interactions, the estimated results of color on art or matte paper can be more accurately approximated. Figure 7 and Table II show the results for maximum ΔE^*_{94} between the original reflectance and the estimated reflectance in 81 color samples for each paper and illuminant. Note that the estimated reflectance is calculated using the best selection of 450, 470, 530, 570, and 610 nm LEDs, which was obtained using illuminant D50 and coated paper. We obtained highly accurate reproduction for illuminants A, C, and D65. Based on Figs. 7(a) and 7(b), it is confirmed empirically that the estimation matrix obtained for coated paper and illuminant D50 is also effective for other types of paper and illuminant.

As a result, we found that the best number of LEDs is five, and the peak wavelengths of LEDs were obtained as 450, 470, 530, 570, and 610 nm, respectively.

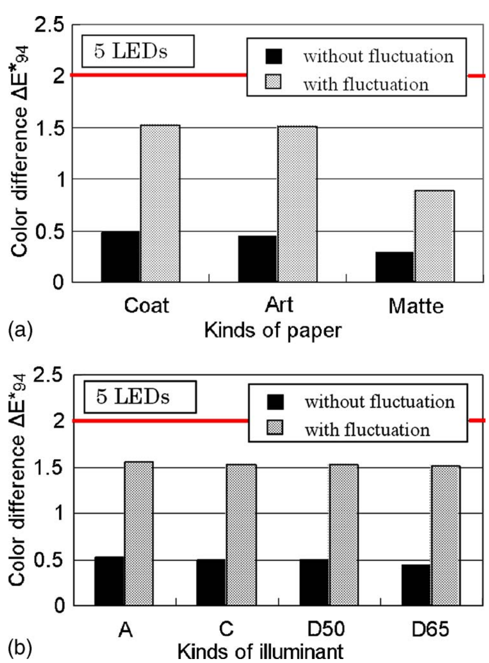

Figure 7. Results of ΔE^*_{94} for each type of paper and illuminant.

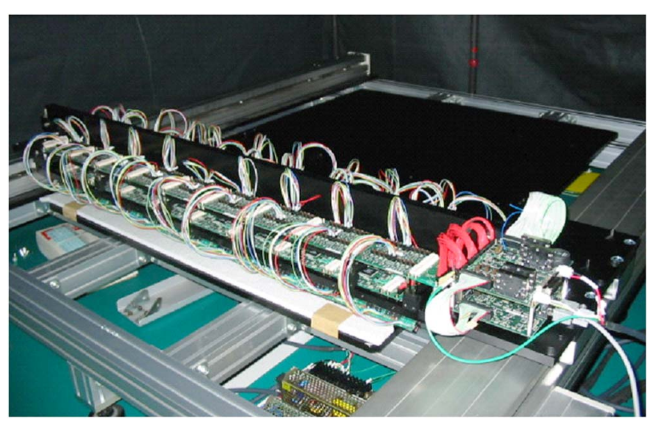

Figure 8. Prototype multi-spectral scanner.

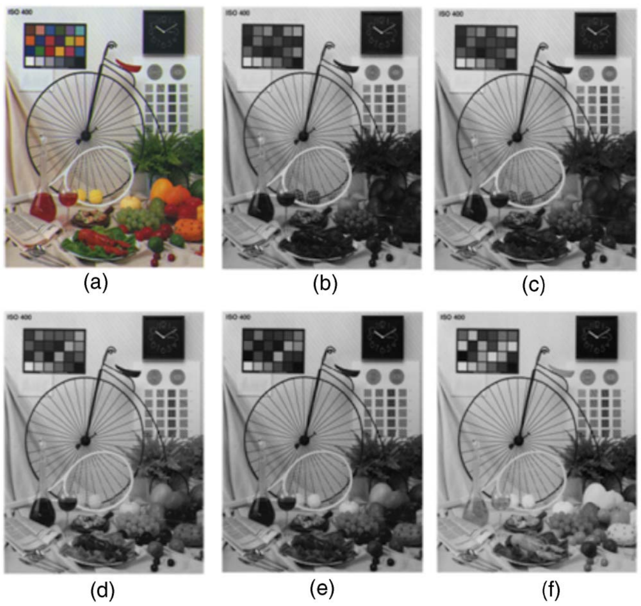

Figure 9. Resulting images measured by the multi-spectral scanner: (a) color proof printed by press, (b) scanned image by a 450 nm LED, (c) scanned image by a 470 nm LED (d) scanned image by a 530 nm LED (e) scanned image by a 570 nm LED (f) scanned image by a 610 nm LED. (Available in color as Supplemental Material on the IS&T website, www.imaging.org.)

DEVELOPMENT OF A MULTI-SPECTRAL SCANNER

We developed a multi-spectral scanner using the best combination of five LEDs. Figure 8 shows a prototype multi-spectral scanner that can measure a 1024 mm × 800 mm print sample, and Fig. 9 (Available in color as Supplemental Material on the IS&T website, www.imaging.org) shows the resulting images that were measured by this scanner. The scanner consists of a sensor head with a detector, LED illuminations, and a processing circuit. The detector has a 2048 photodiode array and an SLA is inserted between the print and the detector. A surface-mount-type LED is used in the scanner in order to make it more compact for practical use.

Thirty-two sets of the five selected LEDs were used as the multi-band illumination. The peak wavelength of all LEDs was measured before mounting, and we used only LEDs that have fluctuations within ±10 nm of the peak wavelength, corresponding to the designed center wavelength. These sets of three LEDs are aligned to illuminate the print from an angle of +45°. We were unable to align five types of LED as one linear array because the power of each LED was insufficient for sparse alignment for each type of LED. Therefore, the remaining LEDs were aligned to illuminate the print from an angle of −45°.

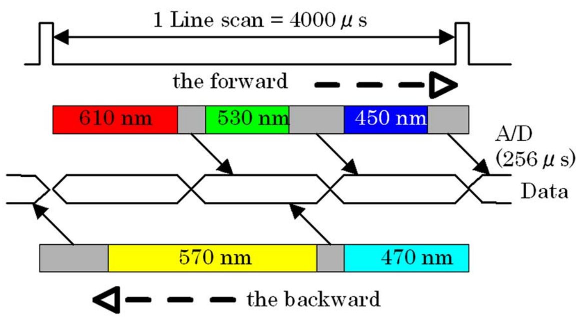

Figure 10. Timing chart of the timesharing process for each LED.

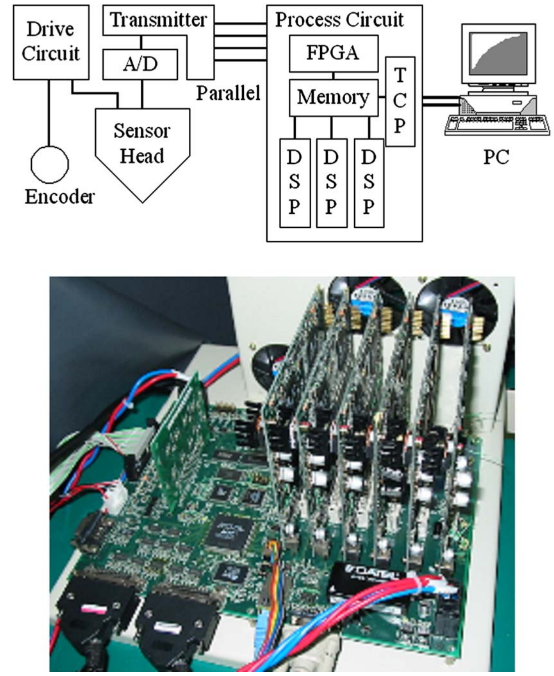

Figure 11. Block diagram and picture of the processing circuit.

In the system, the print is scanned twice: forward and backward. Three types of LED from +45° angles are used for illumination in the forward scan, and two types of LED from −45° angles are used for illumination in the backward scan. Each LED emission is controlled by the timesharing process to illuminate the print by one type of LED at each time. Figure 10 shows the timing chart of the timesharing process. For effective output level setting, the time of the measurement at each line is divided by the ratio of the LED power in order to determine the duration time for each LED.

The scanner is capable of sampling 2048 × 1600 pixels to measure an image of 1024 mm × 800 mm with a pitch of 0.5 mm. A standard white plate is mounted at the home position of the scanner, and the responses of darkness and whiteness are initially measured at the home position. The amplitude fluctuation of each LED is compensated using this initial measurement, as shown in Eq. (1). The analog response of the photodetector for each LED illumination is converted to 16 bits by an A/D converter, and the number of digital data reaches approximately (2048 × 1600 × 5 × 2), corresponding to 33 mb, which is acquired by all of the pixels for each LED. The digital data are sent from the multi-spectral scanner to the processing circuit by a high-speed transmitter. The processing circuit performs the calculations of the calibration and multiple regression method as given by Eqs. (1) and (2).

Figure 11 shows the processing circuit, which is composed of the FPGA, the memory, and the DSP. The calibration of amplitude fluctuation by Eq. (1) is performed at the FPGA in the time series, and the stream of responses is instantly stored in the memory. The calculation of the multiple regression method by Eq. (2) is performed at the DSP, which is superior for handling responses stored in memory. In this calculation, expressed in Eq. (2), we adopt distributed computation using six DSPs, where 342 pixels are assigned to each of the six DSPs.

The scanning speed is designed to require 4000 μs per 0.5 mm pitch based on the architecture of the hardware in the developed multi-spectral scanner. The total number of scans required to measure a proof with a width of 800 mm and a pitch of 0.5 mm is 1600. In this system, approximately 16 s is required for the multi-spectral measurement because the color proof is scanned forward and backward. Therefore, the total measurement time, including calculation and display for practical examination, is less than 20 s.

EVALUATION OF THE DEVELOPED SYSTEM

In this section, we evaluate and discuss the performance of the newly developed multi-spectral scanner. The multiple regression matrix for estimation is determined from the 81 color samples on coated paper, and the spectral reflectances are estimated from the responses for 928 colors in the ISO12642 IT8/3 chart. Figures 12(a) and 12(b) show the examples of estimated reflectance spectra compared to the original reflectance spectra. The best estimation, shown in Fig. 12(a), achieves an acceptable accuracy over the entire wavelength. In contrast, the worst estimation, shown in Fig. 12(b), fails to fit the spectral reflectance in the region, except for the center wavelength of the selected LEDs. In this case, five LEDs are insufficient to represent the spectral pattern.

Figure 12(c) shows the color difference between the original and estimated reflectance spectra of 928 colors charts using the developed multi-spectral scanner. The average color difference ΔE^*_{94} is 1.23, and the maximum color difference ΔE^*_{94} is 4.07. In general, in the printing industry, the empirically acceptable average color difference is approximately 2.5, and the maximum color difference is approximately 3.0 in the CIE $L^*a^*b^*$ color space.[17,18] Therefore, the multi-spectral scanner developed using LEDs is considered to have sufficient accuracy with respect to average color difference, even though the maximum color difference exceeds the value of $\Delta E^*_{94}=3.0$. In the next section, we will improve the estimation method in order to reduce the maximum color difference.

CLUSTERING AND POLYNOMIAL REGRESSION

In this section, the clustering method and polynomial regression method[19] are applied to improve the accuracy of estimation with respect to the maximum color difference. Figure 13(a) shows the CIE a^*b^* diagram of estimated color for 928 samples, which are printed on coated paper and observed under illuminant D50. The estimated color is obtained using the multiple regression method. The triangles indicate the color samples having a color difference greater

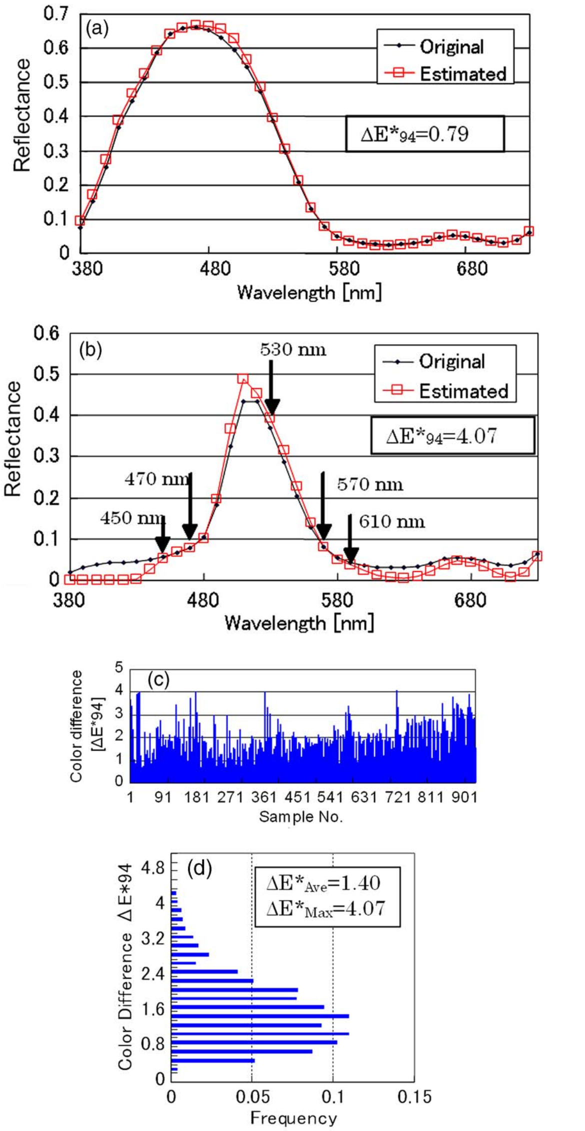

Figure 12. Results of estimation accuracy using the multiple regression method. (a) Best examples of spectral reflectance by estimation. (b) Worst examples of spectral reflectance by estimation (↓ center wavelength of LEDs used herein). (c) Color difference of 928 colors in the IT/8 chart between the original and estimated spectral reflectance. (d) Histogram of the color difference of 928 colors in the IT/8 chart

than $\Delta E^*_{94}=2.5$, and the dots indicate the other color samples. In this diagram, the triangles appeared in the red and green hue regions. Therefore, we apply the clustering method in these regions, which, in this paper, is performed simply by dividing the area by hue angle. For the results that exceed 2.5 with respect to color difference ΔE^*_{94}, the centers of the hue angles for the green and red regions were calculated by the *k*-mean method. In each region, the upper limit of the hue angle is decided by adding the quantity obtained by multiplying the standard deviation of these hue angles by 3 to the center of the hue angle, and the lower limit of the hue angle is decided by subtracting the quantity obtained by multiplying the standard deviation by 3 from the center of the hue angle.

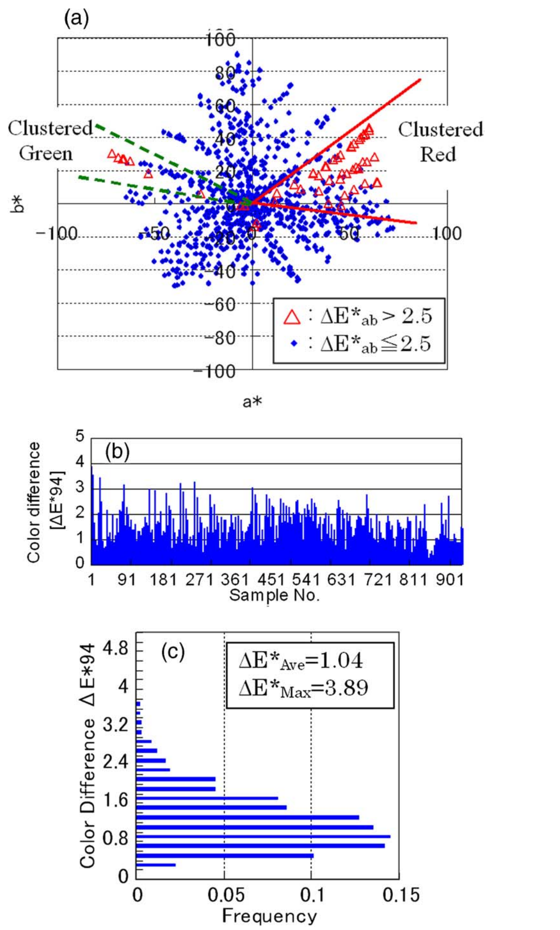

Figure 13. Improved results of estimation accuracy using the clustering method. (a) Results for the estimated spectra in the CIE a^*b^* spaces. (b) Color difference of 928 colors in the IT/8 chart. (c) Histogram of the color difference of 928 colors in the IT/8 chart.

For the clustering method, we first performed a preliminary estimation using 81 samples for training and 928 samples for testing. As shown in Fig. 13(a), based on the obtained results, for the red sample within the angles of −5° to 40° in hue, the angle was classified from the 81 samples, and the green sample within the angles of 145° to 175° was also classified from the 81 samples. As a result, three estimation matrixes were constructed using the clustered red sample, the clustered green sample, and the 81 samples. In practical scanning, the first estimation of 928 samples for testing is executed using a color matrix of all 81 samples, and $L^*a^*b^*$ of the estimated spectral reflectance is calculated. For $L^*a^*b^*$ of the samples included in the red or green cluster area, the estimation is executed again using the corresponding estimation matrix. Figure 13(b) shows the color difference of 928 color samples based on this clustering method. The average color difference is improved to be $\Delta E^*_{94}=1.04$, and the maximum color difference is $\Delta E^*_{94}=3.89$. From these results, the clustering method is considered to be effective for improving the accuracy of estimation for spectral reflectance. However, we could not effectively reduce the maximum color difference using the clustering method.

The polynomial regression method is expected to improve the accuracy of estimation because the error of estimated reflectance is caused by a nonlinear characteristic, which is not expressed by the multiple regression method in Fig. 12(b). This polynomial regression method is performed in order to add the squared response P_i^2 in the calculation of the multiple regression matrix, as shown in Eq. (3),

$$\begin{bmatrix} \hat{R}_{380} \\ \hat{R}_{390} \\ \vdots \\ \hat{R}_{780} \end{bmatrix} = \begin{bmatrix} A_{380,1} & A_{380,2} & \cdots & A_{380,i} & A^2_{380,1} & \cdots & A^2_{380,i} \\ A_{390,1} & \ddots & & & & & \\ \vdots & & & & & & \vdots \\ A_{780,1} & & & & & \cdots & A^2_{780,i} \end{bmatrix} \times \begin{bmatrix} P_1 \\ P_2 \\ \vdots \\ P_i \\ P_1^2 \\ \vdots \\ P_i^2 \end{bmatrix}. \tag{3}$$

For the polynomial regression method, we use an estimation matrix calculated by Eq. (3) with 81 colors, and evaluation is performed using 928 samples. Figure 14(a) shows a comparison of the estimated reflectance spectra calculated by the polynomial regression method and by the multiple regression method. This example is for the same sample as in Fig. 12(b), which is the worst sample using the multiple regression method. The spectral pattern better fits the original reflectance than that obtained by the multiple regression method, and the color difference between the estimated reflectance and the original reflectance is improved using the polynomial regression method.

Figure 14(b) shows the color difference of 928 color samples using the polynomial regression method. The results show that the average and maximum color differences are improved to $\Delta E^*_{94}=1.02$ and $\Delta E^*_{94}=2.84$, respectively.

CONCLUSION

We have developed a multi-spectral scanner using an LED array to construct an accurate digital color proofing system. For the system design, a robust technique was proposed to select LEDs from combinations of 40 commercially available LEDs in order to minimize the color difference ΔE^*_{94} between the measured reflectance and the estimated reflectance. In this selection of LEDs, the fluctuation caused by the epitaxial deposition process during manufacture was taken into account. As a result of LED selection, we found that five LEDs are required in order to estimate spectral reflectance with $\Delta E^*_{94}=2$. The peak wavelengths of the LEDs were selected as 450, 470, 530, 570, and 610 nm and were independent of changes in the illuminant conditions.

For practical verification in the printing industry, we constructed a prototype multi-spectral scanner using the

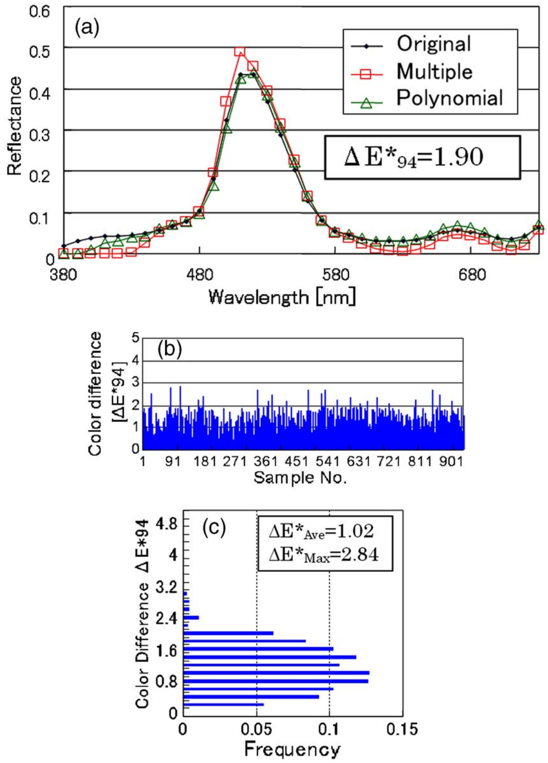

Figure 14. Improved results for estimation accuracy using the polynomial regression method. (a) Example of spectral reflectance estimation. (b) Color difference of 928 colors in the IT/8 chart. (c) Histogram of the color difference of 928 colors in the IT/8 chart.

LED array. In the sensor head, the photodiode array, which has 2048 pixels, was used as a detector, and a Selfoc lens array was inserted for imaging between the object and the detector. In the processing circuit, the FPGA and the DSP were used to accelerate the calculation of sensor calibration and spectral reflectance estimation. The scanner has a pitch resolution of 0.5 mm and a scanning speed of 100 mm/s. In practical evaluation, we found that the measurement was completed within 20 s, including calculation and display.

The spectral reflectance of the 928 color chart is used to evaluate the accuracy of the measurement and the estimation. The estimation procedure was determined by measuring the spectral reflectance of 81 typical color samples. Using the multiple regression method, we found the average color difference was $\Delta E^*_{94}=1.23$ and the maximum color difference was $\Delta E^*_{94}=4.07$. The clustering method and the polynomial regression method were also introduced in order to improve the accuracy of the estimated reflectance spectra compared with the multiple regression method. Among these methods, the polynomial regression method was found to be most effective for practical application in the printing industry because the average color difference was then $\Delta E^*_{94}=1.02$ and the maximum color difference was $\Delta E^*_{94}=2.84$. In the present study, we believe that this multi-spectral scanner system is very significant for obtaining accurate digital color proofs.

ACKNOWLEDGMENTS

This study was supported in part by SCOPE (Strategic Information and Communications R&D Promotion Programme) of the Ministry of Public Management, Home Affairs, Posts and Telecommunications of Japan.

REFERENCES

[1] Printnet: http://www.printnet.com.au/
[2] H. Yamane, "Next generation digital archive system based on super high definition imaging database", *Proc. Electronic Imaging and the Virtual Arts 2000 GIFU*, **14**, 1–7 (2000).
[3] S. Suzuki, T. Kusunoki, and M. Mori, "Color characteristic design for color scanners", Appl. Opt. **29**, 5187–5192 (1990).
[4] G. Sharma and H. J. Trussell, "Set theoretic estimation in color characterization", J. Electron. Imaging **5**, 479–489 (1996).
[5] F. Konig, "Reconstruction of natural spectra from color sensor using nonlinear estimation methods", *Proc. IS&T's 50th Annual Conference* (IS&T, Springfield, VA, 1997) pp. 454–458.
[6] ISO13655, "Graphic technology Spectral measurement and colorimetric computation for graphic arts images" (1996).
[7] International Color Consortium (ICC), "Recommendations for color measurement, White paper #3", http://www.color.org/ICC_white_paper3measurement.pdf
[8] P. D. Burns and R. S. Berns, "Analysis multispectral image capture", *Proc. IS&T/SID 4th Color Imaging Conference* (IS&T, Springfield, VA, 1996) pp. 19–22.
[9] H. Haneishi, T. Hasegawa, A. Hosoi, Y. Yokoyama, N. Tsumura, and Y. Miyake, "System design for accurately estimating the spectral reflectance of art paintings," Appl. Opt. **39**, 6621–6632 (2000).
[10] M. Yamaguchi, T. Teraji, K. Ohsawa, T. Uchiyama, H. Motomura, Y. Murakami, and N. Ohyama, "Color image reproduction based on the multispectral and multiprimary imaging: Experimental evaluation", Proc. SPIE **4663**, 15–26 (2002).
[11] S. Helling, E. Seidal, and W. Biehlig, "Algorithms for spectral color stimulus reconstruction with a seven-channel multispectral camera", *The Second European Conference on Color Graphics Imaging and Vision* (IS&T, Springfield, VA, 2004) pp. 229–262.
[12] J. Y. Hardeberg, F. J. Schmitt, and H. Brettel, "Multispectral image capture using a tunable filter", Proc. SPIE **3963**, 77–88 (1999).
[13] F. H. Imai, M. R. Rosen, and R. S. Berns, "Comparison of spectrally narrow-band capture versus wide-band with priori sample analysis for spectral reflectance estimation", *Proc. IS&T/SID 8th Color Imaging Conference* (IS&T, Springfield, VA, 2000) pp. 234–241.
[14] J. Y. Hardeberg, F. Schmitt, and H. Brettel, "Multispectral color image capture using a liquid crystal tunable filter", Opt. Eng. (Bellingham) **41**, 2532–2548 (2002).
[15] A. Ribes, H. Brettel, F. Schmitt, H. Liang, J. Cupitt, and D. Saunders, "Color and multispectral imaging with the CRISTATEL muitispectral system", *Proc. IS&T's PICS* (IS&T, Springfield, VA, 2003) p. 215.
[16] R. McDonald and K. J. Smith, "CIE94 a new colour-difference formula", J. Soc. Dyers Colour. **111**, 376–379 (1995).
[17] ISO/TC130 Activities and ISO Standards, "The Standardization of Graphic Technology, Japan Printing Machinery Association", May, 2005; http://www.color.org.JapanColor2005English.pdf
[18] ASTM, "Method E 97-53 T" (1953).
[19] N. Tsumura, H. Haneishi, and Y. Miyake, "Estimation of spectral reflectances from multi-band images by multiple regression analysis", Jpn. J. Opt. **27**, 384–391 (1998) (in Japanese).